Active Vibration Control Strategy to Prevent Nonlinearly Coupled Rotor-Stator Whirl Responses in Multi-mode Rotordynamic Systems

Chakkapong Chamroon, Matthew O. T. Cole and Theeraphong Wongratanaphisan

***Abstract*—This paper describes an active control method to prevent unwanted nonlinear vibration response modes of a rotordynamic system. Nonlinear stiffness of components that support or surround a machine rotor can cause a response branch that extends critical vibration (resonance) over a wide interval of rotational speeds. Within this interval, jump transitions between alternative low amplitude and high amplitude response modes become possible. This paper explains how such behavior can be eliminated by applying control forces to the rotor based on dynamic feedback of strains measured in the stator structure. An optimal model-based controller synthesis is considered that combines a Lur'e-type Lyapunov function with a quadratic cost measure to penalize controller gain and bandwidth. Results are presented for an experimental flexible rotor system where nonlinear rotor-stator interaction occurs through a bearing with radial clearance. An active magnetic bearing applies control forces to the rotor in a separate plane. The results show the control technique can eliminate jump response modes and can significantly reduce mechanical stress associated with rub interaction of the rotor and stator. The influence of key parameters in the model and controller formulation are shown.**

***Index Terms*—Rotordynamics, nonlinear vibration, rotor stator rub, magnetic bearing**

I. Introduction

VIBRATION in rotating machines has various causes. These include mass-eccentricity of rotor parts, misalignment of couplings or sleeves, trapped fluid and thermal bends. Typical vibration involves synchronous orbital motions of the rotor around the axis of rotation and is most severe at critical speeds, i.e. when the frequency of rotation coincides with the natural frequency of vibration for a structural mode.

Linear response behavior is a common assumption for rotor balancing procedures as well as established methods for active control of unbalance-induced vibration [1]-[6]. Importantly, however, when bearings or other supporting parts have nonlinear stiffness characteristics (or when radial clearances are present within parts such as bearings, bushes or seals), a jump to a nonlinear vibratory state can occur even when residual excitation of the rotor is relatively low. This paper considers a problematic case of such bistable response behavior. Specifically, it considers how the application of control forces to a rotor can prevent critical states of coupled rotor-stator whirl. For passive systems, an analysis of this problem was first reported by Black [7] and was more recently extended for the case of multiple rotor-stator interaction planes in [8].

Previous work on active control of vibration in nonlinear rotordynamic systems covers quite diverse situations. Unbalance compensation in a single-disk rotor with nonlinear supports was considered in [9]. Adaptive control of synchronous vibration for a rotor supported by magnetic bearings when contacting with touchdown bearings is covered in [10]. The use of actuated clearance bearings has been proposed for alleviating rub interaction [11], and for recovering stable levitation in magnetic bearing systems [12]. In other work, destabilizing nonlinear effects are accounted for in controller designs through linear approximations [13]-[16].

For the control problem considered herein, linearization techniques cannot be applied. Instead, dynamic feedback of measured variables must be used to intrinsically alter the nonlinear dynamics of the system and thereby achieve global stabilization of a desired vibration response mode.

II. Considered Nonlinear Vibration Problem

A flexible or compliantly supported rotor may be prone to contact interaction with surrounding/supporting parts at certain locations along its length, as shown schematically in Fig. 1. Vibration due to unbalance involves lateral deflection of the rotor $\boldsymbol{z}(t)$ with an orbital motion that is synchronous with rotation. Interaction is avoided if the orbit radius satisfies $\rho = \|\boldsymbol{z}\|/c < 1$ where c is the radial clearance. In this situation, however, the possibility of an alternative vibration response mode involving coupled rotor-stator whirl may also exist. This can be shown graphically by a whirl mode map [8]. Fig. 2 shows an example map for a rotor having critical speed Ω_c (for linear vibration). For a given rotational speed Ω, a jump response can occur if ρ exceeds the critical value indicated by the boundary $\Gamma(\Omega)$. Thus, a linear response within region A has the potential to jump to an alternative response within region B. Typical linear response curves C_P and C_Q are also shown in Fig. 2. Curve C_P, which corresponds to unbalance vibration only, avoids region A and is therefore a unique response. For curve C_Q, which corresponds to unbalance plus geometric eccentricity, there is a speed interval where a jump in vibration amplitude from region

Manuscript received ******; accepted ******. Manuscript received in final form ******. This work was supported by the Thailand Research Fund under Grant RSA5280027. C. Chamroon was funded by the Commission on Higher Education of the Royal Thai Government (PhD contract no. 122/2550). Recommended by ********.

C. Chamroon and T. Wongratanaphisan are with the Department of Mechanical Engineering, Chiang Mai University, Chiang Mai 50200, Thailand (e-mail: goffy047@hotmail.com; wong@dome.eng.cmu.ac.th)

M. O. T. Cole is with the Department of Mechanical Engineering, University of Bath, Bath BA2 7AY, UK (e-mail: ensmc@bath.ac.uk)

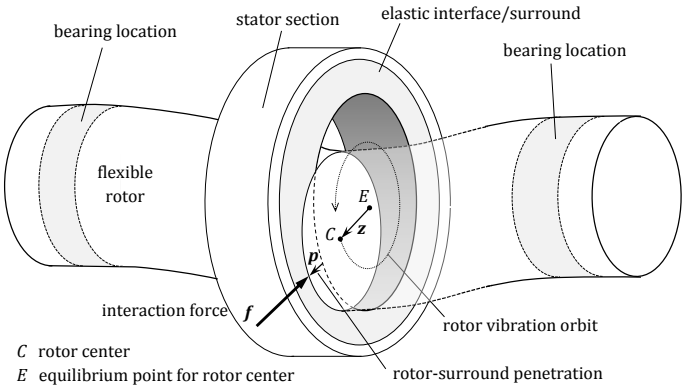

Fig. 1. Schematic diagram of a flexible rotor-stator system showing cross-section where interaction between the rotor and surrounding part occurs

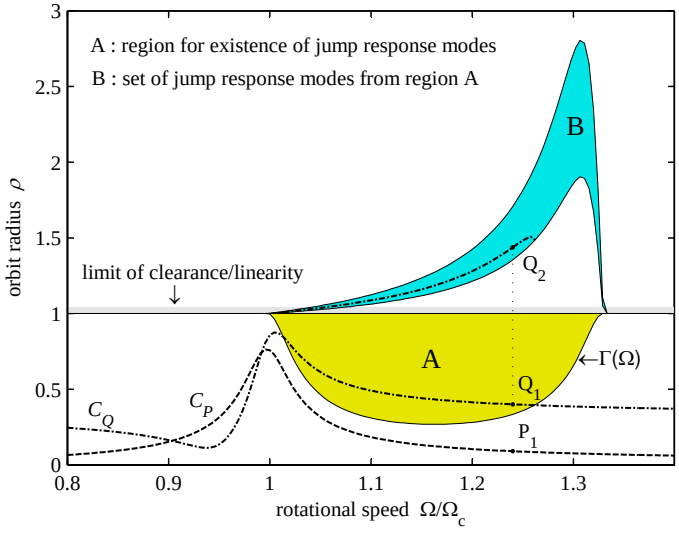

Fig. 2. Illustrative whirl mode map showing potential for nonlinear jump behaviour in rotor synchronous vibration

A to region B is possible. Example degenerate response modes are indicated by points Q_1 and Q_2. Note that a jump transition between alternative response modes must usually involve some transient disturbances acting on the system, examples of which will be given later.

When the system is rotationally symmetric (radially isotropic), a whirl mode map can be calculated directly from frequency response data for the rotor-stator structure. For an initial linear response with orbit radius $\rho < 1$, the magnitude of rotor-stator interaction force for an alternative response mode involving constant rub is given by (see [7] or [8]):

$$\|\boldsymbol{f}\| = \frac{-\cos\angle H(\Omega) + \sqrt{\rho^2 - \sin^2\angle H(\Omega)}}{|H(\Omega)|} \tag{1}$$

Here, $H(\Omega)$ is the dynamic compliance (polar receptance) of the rotor-stator structure in the plane of interaction. A jump response exists only if $\|\boldsymbol{f}\|$ is real and positive, requiring that

$$\rho \geq \sin\angle H(\Omega), \quad \cos\angle H(\Omega) < 0 \tag{2}$$

For a typical multi-mode rotor system, $\cos\angle H(\Omega) < 0$ will hold for a finite speed interval above each critical speed. Region A then has a U-shaped boundary, as seen in Fig. 2.

For machines with active bearings, or some form of active structure, it is possible that controllers can be designed to eliminate the region A (and thus B) so that critical vibration as a nonlinear jump response is avoided. An initial study of this problem considered static feedback control of a magnetic bearing [17]. This approach is not generally applicable to multi-mode systems if actuation forces and nonlinear elements are not collocated. Also, static feedback lacks high frequency attenuation properties and this incurs a risk of control force saturation if hard impacts occur between the rotor and surround.

III. Controller Design

A. Modeling and Controller Formulation

A state-space model for lateral vibration of a rotor-stator structure may be considered in the form:

$$\dot{\boldsymbol{x}} = \boldsymbol{A}\boldsymbol{x} + \boldsymbol{B}_u\boldsymbol{u} + \boldsymbol{B}_f\boldsymbol{f} + \boldsymbol{B}_d\boldsymbol{d} \tag{3}$$

$$\boldsymbol{f} = \beta(\boldsymbol{z}), \quad \boldsymbol{z} = \boldsymbol{C}_z\boldsymbol{x} \tag{4}$$

Here, the state vector $\boldsymbol{x}$ comprises linear displacement and velocity states for the structure in either local or generalized coordinates. The vector $\boldsymbol{u}$ represents control forces applied by active elements, while $\boldsymbol{d}$ models disturbances acting on the structure (nominally unbalance forces). The vector $\boldsymbol{f} = [f_x\ f_y]^T$ represents internal forces used to model nonlinear interaction of the rotor and surround. These forces are assumed to arise at an interface/component having elastic properties and so depend on local relative displacement states $\boldsymbol{z} = [z_x\ z_y]^T$ through a static (time-invariant) mapping $\beta : \mathbb{R}^2 \to \mathbb{R}^2$. A linear model with the form (3) can be derived theoretically using finite element techniques, which are well-covered in the rotordynamics literature (see [18] or [19]). Note that (3) and (4) may also be appropriate for an actively controlled system if linear controller dynamics are incorporated in (3). In what follows it will be assumed that the 'uncontrolled' linearized model ((3) with $\boldsymbol{f} = 0$) is stable, i.e. $\boldsymbol{A}$ is a stability matrix.

To further specify β it will be assumed that, within the plane of interaction, both the rotor and surround are circular in cross-section. A vector is then defined for the rotor radial deflection (penetration) beyond the clearance, as shown in Fig. 1:

$$\boldsymbol{p} = \begin{cases} 0, & \|\boldsymbol{r}\| \leq c \\ (1 - c/\|\boldsymbol{r}\|)\boldsymbol{r}, & \|\boldsymbol{r}\| > c \end{cases} \tag{5}$$

where $\boldsymbol{r} = \boldsymbol{z} + \boldsymbol{e}$, with $\boldsymbol{e}$ being the fixed position of the rotor equilibrium point relative to the clearance circle center. Adopting a general compliant contact model, the interaction force may be defined in terms of a bounded stiffness relation:

$$\boldsymbol{f} = -\kappa(\|\boldsymbol{p}\|)\boldsymbol{p}, \quad 0 \leq \kappa(\|\boldsymbol{p}\|) < k \tag{6}$$

Thus, k specifies an upper bound for $\|\boldsymbol{f}\|/\|\boldsymbol{p}\|$. Further discussion of this type of nonlinear interaction model and its effect on rotor vibration behavior can be found in [8] and [19].

It can be verified using (5) and (6) that, provided $\|\boldsymbol{e}\| < c$, the following constraint holds whenever $\boldsymbol{f} \neq 0$:

$$\boldsymbol{f}^T\boldsymbol{f} + k\boldsymbol{f}^T\boldsymbol{z} < 0 \tag{7}$$

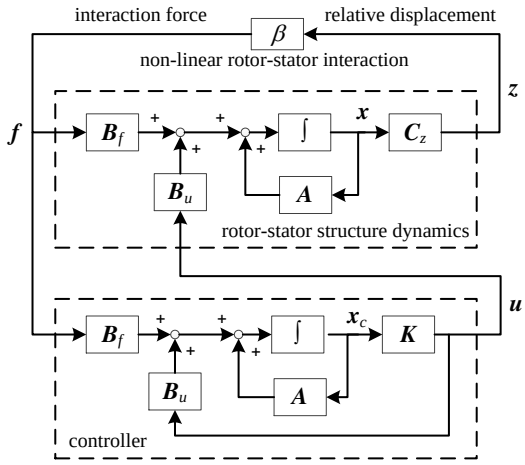

Fig. 3. Control scheme based on feedback of rotor-stator interaction forces

As it is difficult to treat the nonlinear relations (5) and (6) explicitly within a controller design procedure, the constraint (7) may be used in an alternative approach [19]: if stability can be established subject to (7), it is also implied for the specific case defined by (5) and (6).

Consider now the structure in Fig. 3 with controller

$$\begin{array}{rcl} \dot{\boldsymbol{x}}_c & = & (\boldsymbol{A}+\boldsymbol{B}_u\boldsymbol{K})\boldsymbol{x}_c+\boldsymbol{B}_f\boldsymbol{f} \\ \boldsymbol{u} & = & \boldsymbol{K}\boldsymbol{x}_c \end{array} \tag{8}$$

For this form of controller, the states $\boldsymbol{x}_c$ can be viewed as estimates of the components of $\boldsymbol{x}$ due to the interaction force $\boldsymbol{f}$. Note that implementation requires that measurement, or inference, of the interaction force is possible. This will be discussed later. The controlled dynamics are given by (4) and

$$\left[\begin{array}{c} \dot{\boldsymbol{x}} \\ \dot{\boldsymbol{w}} \end{array}\right] = \left[\begin{array}{cc} \boldsymbol{A}+\boldsymbol{B}_u\boldsymbol{K} & -\boldsymbol{B}_u\boldsymbol{K} \\ \boldsymbol{0} & \boldsymbol{A} \end{array}\right]\left[\begin{array}{c} \boldsymbol{x} \\ \boldsymbol{w} \end{array}\right]+\left[\begin{array}{c} \boldsymbol{B}_f \\ \boldsymbol{0} \end{array}\right]\boldsymbol{f} \tag{9}$$

where $\boldsymbol{w}=\boldsymbol{x}-\boldsymbol{x}_c$. Given that $\boldsymbol{A}$ is a stability matrix, $\boldsymbol{w}$ will converge to zero. Therefore, a stability-performance analysis can be based on the following reduced-order model:

$$\begin{array}{rcl} \dot{\boldsymbol{x}} & = & (\boldsymbol{A}+\boldsymbol{B}_u\boldsymbol{K})\boldsymbol{x}+\boldsymbol{B}_f\boldsymbol{f} \\ \boldsymbol{f} & = & \beta(\boldsymbol{z}), \quad \boldsymbol{z}=\boldsymbol{C}_z\boldsymbol{x} \\ \boldsymbol{y} & = & \boldsymbol{C}_y\boldsymbol{x} \end{array} \tag{10}$$

The output $\boldsymbol{y}$ is defined for the purpose of controller design and includes weighted components of vibration states and control forces:

$$\boldsymbol{y}=\left[\begin{array}{c} \alpha\boldsymbol{z} \\ \boldsymbol{u} \end{array}\right] \Rightarrow \boldsymbol{C}_y=\left[\begin{array}{c} \alpha\boldsymbol{C}_z \\ \boldsymbol{K} \end{array}\right] \tag{11}$$

The scalar $\alpha \geq 0$ may be selected in the design.

Although alternative, and more general, feedback control structures could be considered, the scheme described here has a number of attractive features. Firstly, the use of direct measurements of the contact force circumvents the need for an exact nonlinear model for rotor-stator interaction. In addition:

1) The estimator-based design leads to reduced-order stability analysis and controller synthesis problems.
2) The parametrization (and synthesis) of controller solutions is made over the gain matrix $\boldsymbol{K}$.
3) The linear part of the system dynamics has a feed-forward structure and is intrinsically stable.
4) The controller acts only when limits of linear behavior are exceeded. Therefore, an initial system/controller design can be made based on linear operation and the globally stabilizing controller applied in parallel without affecting performance during linear operation.

The following subsections deal with how to obtain a suitable stabilizing gain matrix $\boldsymbol{K}$ for the proposed controller. Section III.B develops mathematical conditions for global stability of a fixed equilibrium point for the controlled system (10). These conditions may be viewed as minimum requirements for stability. However, they do not guarantee global stability of a forced response, which must be established if the possibility of a jump response is also to be eliminated. Therefore, section III.C extends the stability conditions to the case of global stabilization of a periodic forced response. These are the actual conditions used in the synthesis of the controller gain $\boldsymbol{K}$.

B. Conditions for Global Stability of a Fixed Equilibrium

The controller design will be made subject to minimization of the generalized $\mathcal{H}_2$ norm of the nonlinear system (10). This is evaluated as the worst-case $\boldsymbol{L}_2$ norm of the output signal $\boldsymbol{y}$ over a specified set of initial values for the state vector (arising nominally due to the injection of impulse disturbances when $t=0$). The norm-bound condition $\|\boldsymbol{y}\|_2<\gamma$ holds if

$$\lim_{\tau\to\infty}\int_0^\tau \boldsymbol{y}^T\boldsymbol{y}\,\mathrm{d}t<\gamma^2 \tag{12}$$

It is well known that this condition holds if there exists a Lyapunov function $V(\boldsymbol{x})$ satisfying [20], [21]

$$\dot{V}(\boldsymbol{x})+\boldsymbol{y}^T\boldsymbol{y}<0 \quad \forall \boldsymbol{x}\neq 0 \tag{13}$$

$$V(\boldsymbol{x}(0))<\gamma^2 \tag{14}$$

A Lyapunov function will be considered in the form

$$V(\boldsymbol{x})=\boldsymbol{x}^T\boldsymbol{P}\boldsymbol{x}-2\nu\int_0^{\boldsymbol{z}}\boldsymbol{f}^T\mathrm{d}\boldsymbol{z} \tag{15}$$

This function combines a quadratic term in the system states with a 2-dimensional Lur'e-type term associated with the elastic energy storage at the rotor-stator contact (as proposed in [19]). The condition $V(\boldsymbol{x})>0, \boldsymbol{x}\neq 0$ holds if $\boldsymbol{P}=\boldsymbol{P}^T>0$ and $\nu\geq 0$. These parameters must be determined so that (13) and (14) are also satisfied. To account for the nonlinear relation between $\boldsymbol{f}$ and $\boldsymbol{z}$, the constraint (7) may be augmented with the constraint (13) via the scalar $\mathcal{S}-$procedure [20]. The resulting requirement is that $\sigma>0$ exists such that

$$\dot{V}(\boldsymbol{x})-2\sigma(k^{-1}\boldsymbol{f}^T\boldsymbol{f}+\boldsymbol{f}^T\boldsymbol{z})+\boldsymbol{y}^T\boldsymbol{y}<0 \quad \forall\left[\begin{array}{c} \boldsymbol{x} \\ \boldsymbol{f} \end{array}\right]\neq 0 \tag{16}$$

where $\dot{V}(\boldsymbol{x})=\dot{\boldsymbol{x}}^T\boldsymbol{P}\boldsymbol{x}+\boldsymbol{x}^T\boldsymbol{P}\dot{\boldsymbol{x}}-2\nu\boldsymbol{f}^T\dot{\boldsymbol{z}}$.

The stability condition (16) has the quadratic form

$$\left[\begin{array}{c} \boldsymbol{x} \\ \boldsymbol{f} \end{array}\right]^T\mathbb{M}_0\left[\begin{array}{c} \boldsymbol{x} \\ \boldsymbol{f} \end{array}\right]<0 \quad \forall\left[\begin{array}{c} \boldsymbol{x} \\ \boldsymbol{f} \end{array}\right]\neq 0 \tag{17}$$

which is equivalent to

$$\mathbb{M}_0 = \left[\begin{array}{cc} \boldsymbol{M}_{11} & \boldsymbol{M}_{12} \\ \boldsymbol{M}_{21} & \boldsymbol{M}_{22} \end{array} \right] < 0 \tag{18}$$

where, with the assumption $\boldsymbol{C}_z\boldsymbol{B}_u = 0$,
$\boldsymbol{M}_{11} = \boldsymbol{P}(\boldsymbol{A}+\boldsymbol{B}_u\boldsymbol{K})+(\boldsymbol{A}+\boldsymbol{B}_u\boldsymbol{K})^T\boldsymbol{P}+\boldsymbol{K}^T\boldsymbol{K}+\alpha^2\boldsymbol{C}_z^T\boldsymbol{C}_z$,
$\boldsymbol{M}_{21} = \boldsymbol{M}_{12}^T = \boldsymbol{B}_f^T\boldsymbol{P}^T - \nu\boldsymbol{C}_z\boldsymbol{A} - \sigma\boldsymbol{C}_z$, $\boldsymbol{M}_{22} = -2\sigma k^{-1}\boldsymbol{I}$.

For a given initial condition $\boldsymbol{x}(0) = \boldsymbol{x}_0$, assumed to be interaction-free (i.e. $\boldsymbol{f}(0) = 0$), we have $V(\boldsymbol{x}_0) = \boldsymbol{x}_0^T\boldsymbol{P}\boldsymbol{x}_0$. Therefore, from (14), the $\mathcal{H}_2$ gain-bound is satisfied if

$$\boldsymbol{x}_0^T\boldsymbol{P}\boldsymbol{x}_0 - \gamma^2\boldsymbol{I} < 0 \tag{19}$$

C. Conditions for Global Stability of a Steady Orbit

In this section we consider that there is some system response $\boldsymbol{x}_d(t)$ arising due to the disturbances $\boldsymbol{d}(t)$ and that this response is contact-free. Thus, $\boldsymbol{x}(t) = \boldsymbol{x}_d(t)$ satisfies (3)-(4) with $\boldsymbol{f}(t) = 0$. We will now derive conditions that can determine whether this response is also globally stable, thereby eliminating the possibility of an alternative (jump) response for which $\boldsymbol{f}(t) \neq 0$. This requires that all state trajectories converge to $\boldsymbol{x}_d(t)$ (including trajectories for which $\boldsymbol{f} \neq 0$). Defining $\boldsymbol{X}(t) = \boldsymbol{x}(t) - \boldsymbol{x}_d(t)$ and $\boldsymbol{W}(t) = \boldsymbol{w}(t) - \boldsymbol{x}_d(t)$, the global dynamics of the controlled system are given by

$$\left[\begin{array}{c} \dot{\boldsymbol{X}} \\ \dot{\boldsymbol{W}} \end{array} \right] = \left[\begin{array}{cc} \boldsymbol{A}+\boldsymbol{B}_u\boldsymbol{K} & -\boldsymbol{B}_u\boldsymbol{K} \\ \boldsymbol{0} & \boldsymbol{A} \end{array} \right] \left[\begin{array}{c} \boldsymbol{X} \\ \boldsymbol{W} \end{array} \right] + \left[\begin{array}{c} \boldsymbol{B}_f \\ \boldsymbol{0} \end{array} \right] \boldsymbol{f}$$
$$\boldsymbol{f} = \beta(\boldsymbol{z}), \quad \boldsymbol{z} = \boldsymbol{C}_z\boldsymbol{X} + \boldsymbol{z}_d \tag{20}$$

where $\boldsymbol{z}_d(t) = \boldsymbol{C}_z\boldsymbol{x}_d(t)$.

Although the system defined by (20) is time-varying (due to the dependence of $\boldsymbol{z}(t)$ on $\boldsymbol{z}_d(t)$), Lyapunov's direct method can still be readily applied [21]. To establish global stability of $\boldsymbol{x}_d(t)$, meaning that $\boldsymbol{X}(t) \to 0$, $t \to \infty$ for all $\boldsymbol{X}(0) = \boldsymbol{X}_0$, a Lyapunov function is defined in the form

$$V(t, \boldsymbol{X}) = \boldsymbol{X}^T\boldsymbol{P}\boldsymbol{X} - 2\nu\int_{\boldsymbol{z}_d}^{\boldsymbol{z}} \boldsymbol{f}^T \,\mathrm{d}\boldsymbol{z} \tag{21}$$

So that

$$\dot{V}(t, \boldsymbol{X}) = \boldsymbol{X}^T\boldsymbol{P}\dot{\boldsymbol{X}} + \dot{\boldsymbol{X}}^T\boldsymbol{P}\boldsymbol{X} - 2\nu\boldsymbol{f}^T\dot{\boldsymbol{z}} \tag{22}$$

Here, the variable $\dot{\boldsymbol{z}}$ depends on both $\boldsymbol{X}$ and $\boldsymbol{z}_d(t)$. It can be shown (see Appendix A) that if $\boldsymbol{z}_d$ is a circular orbit then, for the form of β defined by equations (5) and (6),

$$\boldsymbol{f}^T\dot{\boldsymbol{z}} = \boldsymbol{f}^T(\boldsymbol{C}_z\dot{\boldsymbol{X}} + \Omega\boldsymbol{\Pi}\boldsymbol{C}_z\boldsymbol{X}), \quad \boldsymbol{\Pi} = \left[\begin{array}{cc} 0 & 1 \\ -1 & 0 \end{array} \right] \tag{23}$$

Similar to the procedure in Section III.C, the basic stability condition $\dot{V}(t, \boldsymbol{X}) < 0$ can be combined with the constraint (7) and the $\mathcal{H}_2$ norm-bound (12) to give the condition

$$\mathbb{N}_0(\Omega) = \left[\begin{array}{cc} \boldsymbol{N}_{11} & \boldsymbol{N}_{12} \\ \boldsymbol{N}_{21} & \boldsymbol{N}_{22} \end{array} \right] < 0, \tag{24}$$

$\boldsymbol{N}_{11} = \boldsymbol{P}(\boldsymbol{A}+\boldsymbol{B}_u\boldsymbol{K})+(\boldsymbol{A}+\boldsymbol{B}_u\boldsymbol{K})^T\boldsymbol{P}+\boldsymbol{K}^T\boldsymbol{K}+\alpha^2\boldsymbol{C}_z^T\boldsymbol{C}_z$,
$\boldsymbol{N}_{21} = \boldsymbol{N}_{12}^T = \boldsymbol{B}_f^T\boldsymbol{P}^T - \nu(\boldsymbol{C}_z\boldsymbol{A} + \Omega\boldsymbol{\Pi}\boldsymbol{C}_z) - \sigma\boldsymbol{C}_z$,
$\boldsymbol{N}_{22} = -2\sigma k^{-1}\boldsymbol{I}$.

To allow a controller solution to be obtained using standard LMI solvers, bilinear terms can first be eliminated from (24), as detailed in Appendix B. The resulting condition is

$$\widetilde{\mathbb{N}}_0(\Omega) = \left[\begin{array}{ccc} \widetilde{\boldsymbol{N}}_{11} & \widetilde{\boldsymbol{N}}_{12} & \widetilde{\boldsymbol{N}}_{13} \\ \widetilde{\boldsymbol{N}}_{21} & \widetilde{\boldsymbol{N}}_{22} & \widetilde{\boldsymbol{N}}_{23} \\ \widetilde{\boldsymbol{N}}_{31} & \widetilde{\boldsymbol{N}}_{32} & \widetilde{\boldsymbol{N}}_{33} \end{array} \right] < 0, \tag{25}$$

$\widetilde{\boldsymbol{N}}_{11} = \boldsymbol{A}\boldsymbol{S} + \boldsymbol{S}\boldsymbol{A}^T - \boldsymbol{B}_u\boldsymbol{B}_u^T$,
$\widetilde{\boldsymbol{N}}_{21} = \widetilde{\boldsymbol{N}}_{12}^T = \zeta\boldsymbol{B}_f^T - \eta(\boldsymbol{C}_z\boldsymbol{A} + \Omega\boldsymbol{\Pi}\boldsymbol{C}_z)\boldsymbol{S} - \boldsymbol{C}_z\boldsymbol{S}$,
$\widetilde{\boldsymbol{N}}_{22} = -2\zeta k^{-1}\boldsymbol{I}$, $\widetilde{\boldsymbol{N}}_{31} = \widetilde{\boldsymbol{N}}_{13}^T = \boldsymbol{C}_z\boldsymbol{S}$, $\widetilde{\boldsymbol{N}}_{33} = -\alpha^{-2}\boldsymbol{I}$.

For a nominal angular speed Ω, the optimal controller is found by solving the following LMI optimization problem:

Controller synthesis problem. Minimize γ over $\boldsymbol{S}$, ζ and η subject to $\boldsymbol{S} = \boldsymbol{S}^T > 0$, $\zeta > 0$, $\eta > 0$, $\widetilde{\mathbb{N}}_0(\Omega) < 0$ and

$$\left[\begin{array}{cc} -\gamma^2\boldsymbol{I} & \boldsymbol{X}_0^T \\ \boldsymbol{X}_0 & -\boldsymbol{S} \end{array} \right] < 0.$$

From the solution to this problem, the optimal controller gain is calculated as $\boldsymbol{K}^* = -\boldsymbol{B}_u^T\boldsymbol{S}^{-1}$.

IV. Test System

A. Experimental Rotor-AMB System

An experimental flexible rotor system has been constructed for testing and evaluating active vibration control methods (Fig. 4). The rotor consists of a 10 mm diameter shaft of length 700 mm supported by ball bearings at both ends. Two disks are mounted on the shaft. An active magnetic bearing (AMB) is located at disk 1 (0.36 kg). Disk 2 (1.12 kg) may undergo contact interaction with a surrounding stator part having mass 0.40 kg and compliantly supported by four horizontal rods (Fig. 5(a)). A ball bearing with radial clearance of 600 μm to the stator is fitted on disk 2, the main purpose of which is to reduce tangential friction force at the rotor-stator interface and thereby prevent friction-driven response modes (which are not the focus of the present study). A flexible coupling connects the shaft to a timing pulley and belt, driven by a d.c. motor. The designed speed range is 0-3,600 rpm (0-60 Hz). Non-contact displacement sensors are installed to measure rotor lateral vibration at both disks. Synchronous vibration is associated with physical unbalance of the two disks. Although the exact unbalance condition is unknown, eccentricity of each disk is of the order of 100 μm ($\sim 20\%$ of the clearance).

The AMB is a standard design having opposing pole pairs with coils driven by PWM switching amplifiers. Proportional and derivative feedback of displacements measured at disk 1 is used to overcome the negative stiffness characteristics of the bearing and achieve moderate damping of rotor flexure. The AMB is used to apply additional control forces from the globally stabilizing feedback controller. These forces are limited to below 15 N to ensure linear operation of the AMB.

B. Interaction Force Sensing Device

As the proposed control strategy requires measurements of rotor-stator interaction forces, a specially designed contact

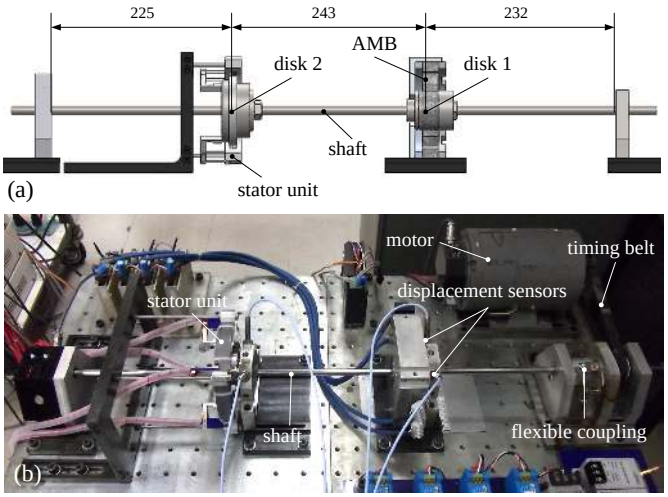

Fig. 4. Experimental rotor-AMB system (a) CAD model (b) Photograph

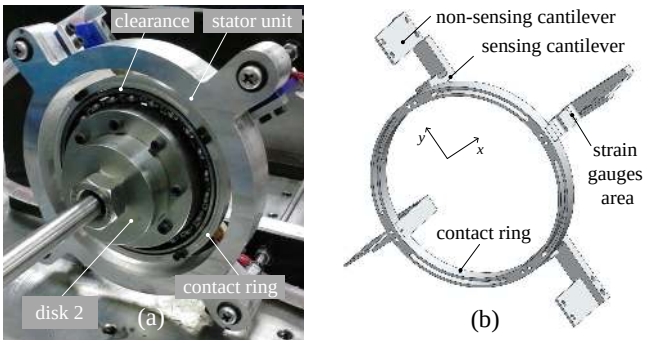

Fig. 5. Contact force sensing device (a) Photograph (b) CAD model

force sensor was manufactured and fitted within the stator unit. This device consists of a contact ring (having clearance to rotor) mounted on four sensing elements, as shown in Fig. 5. Each sensing element consists of one cantilever with strain gauges, connected in series with another cantilever designed to give compliance to the element in an orthogonal (non-sensing) direction. The four sensing elements are arranged circumferentially in opposing pairs to maximize symmetry of the device. Measured strains are converted to lateral (x-y) force components via a linear transformation (identified by calibration procedures). The contact ring and sensing elements are designed to have low mass in order to maximize bandwidth of the device, which is limited by the natural modes of vibration of the contact ring. Finite element modeling was used to optimize sensitivity of the device while maintaining a sufficiently high natural frequency (> 400 Hz). The maximum force that the device can withstand is estimated to be 50 N.

V. Numerical Analysis and Simulation Results

The results in this section are based on a numerical model of the test rig defined in the form of (3)-(6). Model parameters were determined using frequency response data for the rotor and stator structures obtained by impact tests. The resulting state-space model has a total of twelve states and includes first and second modes of vibration of the rotor (with natural frequencies of 22 Hz and 75 Hz and damping ratios of

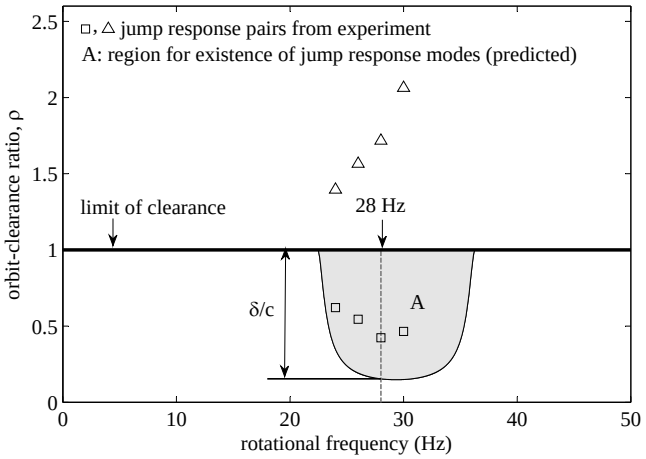

Fig. 6. Whirl mode map for test rig calculated from model. Region A is calculated from $H(\Omega)$, as given by equation (26)

0.023 and 0.024 respectively). The stator is modeled as a compliantly supported lumped mass with natural frequency of vibration 120 Hz and damping ratio 0.008. It is important to recognize that all three structural modes contribute to the dynamic response during rotor-stator interaction and must be accounted for in the controller design. The contact stiffness for rotor-stator interaction κ depends on the radial stiffness of the force-sensor, which is estimated to be 39 kN/m (although only an upper limit is required for the controller synthesis).

For the uncontrolled system, the dynamic compliance of the rotor-stator structure $H(\Omega)$ can be calculated according to

$$H(\Omega) = \left[\begin{array}{cc} 1 & 0 \end{array}\right] \boldsymbol{T}(j\Omega) \left[\begin{array}{cc} 1 & -j \end{array}\right]^T + k^{-1} \qquad (26)$$

where $\boldsymbol{T}(j\Omega) = \boldsymbol{C}_z \left(j\Omega \boldsymbol{I} - \boldsymbol{A}\right)^{-1} \boldsymbol{B}_f$. From equations (2), calculation of the whirl mode map shown in Fig. 6 is then possible. This indicates that a jump response is possible for rotational frequencies between 22 and 37 Hz.

Controllers were synthesized using the methodology described in Section III. A fixed operating speed of 28 Hz was considered for the synthesis, which falls within the predicted interval for jump response. Predicted performance of the controllers can be seen clearly from the hysteresis plots in Fig. 7. These show how the rotor vibration changes as the level of unbalance disturbance is slowly increased and then decreased. For the uncontrolled system there is a large jump in amplitude when the orbit radius first exceeds the clearance. The jump response persists until unbalance returns to a low level. The interval where two possible response modes can occur is indicated by δ. This corresponds to the vertical extent of region A, as shown in Fig. 6. Three different controllers were synthesized with different values of the output weighting α, but using the same value for the contact stiffness bound ($k = 4 \times 10^4$ N/m). All the controllers eliminate jump response behavior for operation at 28 Hz and, though not shown, completely eliminate region A of the whirl mode map.

To demonstrate how a jump response can occur in the uncontrolled system, results from time-step simulation are shown in Fig. 8(a). These results are for steady operation at a frequency of 28 Hz. The rotor unbalance disturbance

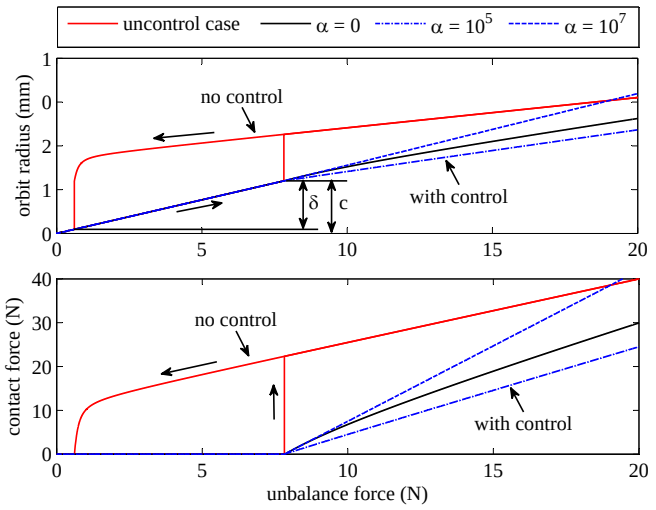

Fig. 7. Variation of orbit radius and contact force with unbalance level for simulated steady-state operation at 28 Hz.

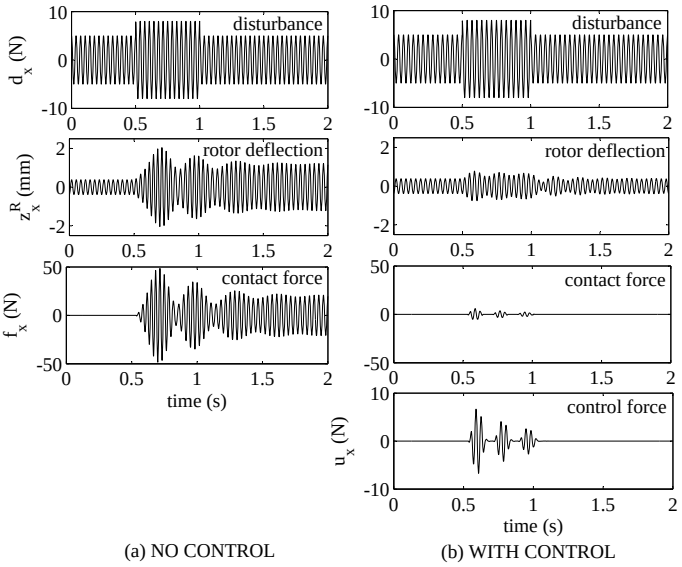

Fig. 8. Simulation of transient behaviour at 28 Hz. Graphs show rotor vibration and contact forces during a temporary increase in unbalance: (a) Uncontrolled case (b) Controlled case

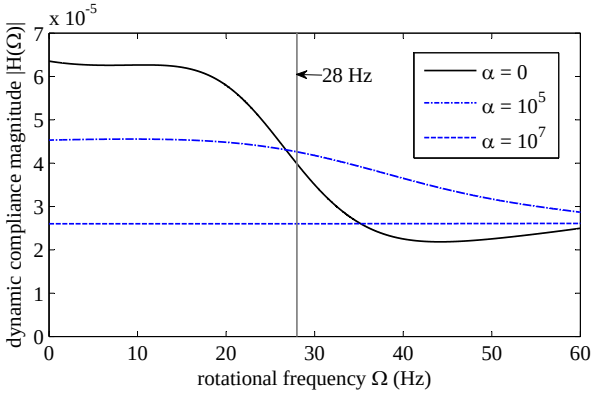

Fig. 9. Dynamic compliance $H(\Omega)$ for the controlled system. The design parameter α has an important influence on the magnitude of this function.

$\boldsymbol{d}$ is initially at a low level so that rotor vibration is well within clearance limits. A temporary increase in unbalance after 0.5 seconds causes rotor-stator contacts and this results in a jump to high amplitude vibration involving coupled rotor-stator whirl. The unbalance force returns to the original level after a further 0.5 seconds, but the coupled whirl response persists indefinitely. In the controlled case (Fig. 8(b)), the jump response is prevented and the level of contact forces during interaction is greatly diminished.

Although, in this study, a temporary increase in unbalance disturbance is used to induce a jump response, other situations can produce the same outcome. For example, an impulsive disturbance applied to the stator structure or motion of the system foundation have the potential to cause rotor-stator contacts leading to sustained coupled whirl. Even when operating active unbalance control strategies [1]-[6], if there is a sudden change in unbalance of the rotor (e.g. due to a blade-loss event) then it may not be possible to suppress the initial vibration sufficiently to prevent rotor-stator contacts.

Figure 7 indicates that the value of α used in the controller synthesis influences the level of contact force when interaction occurs. To explain this influence, the basic equation for jump response prediction (1) may be considered. The existence of a jump solution depends on the phase of $H(\Omega)$. However, when contact is unavoidable ($\rho > 1$), the steady-state contact force depends on the magnitude of $H(\Omega)$. As the design weighting α is used to penalize $\|\boldsymbol{z}\|$, increasing α tends to reduce the magnitude of $H(\Omega)$ and thus give larger contact forces.

The dynamic compliance magnitudes $|H(\Omega)|$ for controllers synthesized with different values of α are presented in Fig. 9. These are calculated from the transfer function matrix $\boldsymbol{T}(j\Omega) = \boldsymbol{C}_z \left(j\Omega \boldsymbol{I} - \boldsymbol{A} - \boldsymbol{B}_u \boldsymbol{K}\right)^{-1} \boldsymbol{B}_f$. The plots confirm that, for the selected frequency, $|H(\Omega)|$ is highest with $\alpha = 10^5$. Although all these controllers have low pass properties, increasing α also tends to increase bandwidth and gain. For a thorough design procedure it would be recommended that α and k are considered as design variables, with suitable values selected by analysis and simulation. For the results in the remainder of the paper, the controller designs were based on $\alpha = 0$ and $k = 4 \times 10^4$ N/m.

VI. Experimental Results

A. Results for Supercritical Operation

Experimental results for identification of the hysteresis behavior during increasing and decreasing unbalance are shown in Fig. 10. Separate graphs show uncontrolled and controlled cases. For these tests, the rotor was operating at a constant rotational frequency of 28 Hz and a simulated unbalance force applied using the magnetic bearing. This acts in addition to the physical unbalance of the rotor. For the uncontrolled case (Fig. 10(a)), the interval for occurrence of a jump response δ is smaller than predicted but, overall, the results show reasonable agreement with the simulations (Fig. 7). The jump response can occur at low levels of excitation but causes high levels of contact forces. The results for operation with control indicate

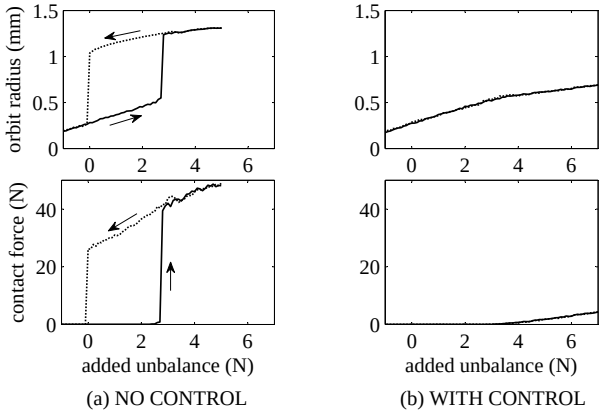

Fig. 10. Variation of orbit radius and contact force with unbalance level for experiments with steady-state operation at 28 Hz. (a) Uncontrolled case (b) Controlled case ($\alpha = 0$)

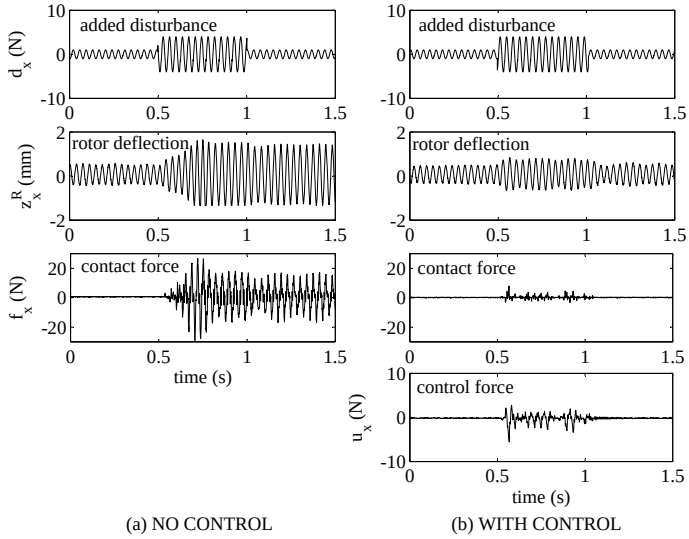

Fig. 11. Experimental transient test at 28 Hz involving temporary increase in unbalance: (a) Uncontrolled case (b) Controlled case

that the jump response is eliminated and that steady-state interaction forces are much lower than without control.

Figure 11 shows experimental results for transient response tests that aim to replicate the time-step simulations of Fig. 8. In practice, the controller was effective in preventing a jump to the alternative whirl response that occurred without control. Discrepancies between the experimental and simulation results are believed to be due mainly to the non-isotropic properties of the experimental system. In particular, the magnetic bearing and force sensing device have a cartesian structure which introduces some radial anisotropy. This causes fluctuations in the radial force during rub between the rotor and stator, which is different to the smooth continuous rub seen in the simulations. An additional cause of inaccuracy may be the idealized nonlinear interaction equations (5) and (6). Importantly, however, the controller synthesis involves a robust approach in the sense that an exact model of rotor-stator interaction is not used and this is believed to contribute to the good control performance seen in the experiments.

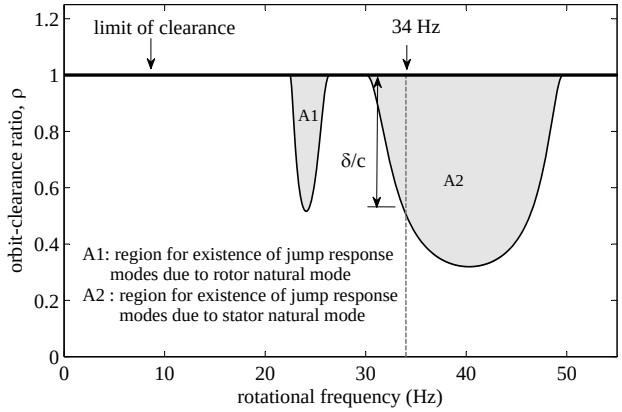

Fig. 12. Whirl mode map for test rig with modified stator dynamics (low frequency stator natural mode)

B. Results with Modified Stator Dynamics

It is important to verify that the proposed control technique can deal with instabilities associated with structural modes of the stator, as well as those of the rotor. As control forces are not applied directly to the stator, the stator dynamics are not controllable by feedback. Nonetheless, the presence of a stator mode with natural frequency within the running speed range can lead to amplitude jump and coupled whirl. To investigate this issue experimentally, mass was added to the stator unit and the supporting rods extended so that the stator mode natural frequency decreased from 120 Hz to 30 Hz. For this situation, two operating ranges are predicted for possible jump response, as shown by the whirl mode map in Fig. 12. The smaller region (A1) is associated with the rotor natural mode while the larger region (A2) is associated with the stator natural mode.

Controllers were designed based on the modified system dynamics and evaluated by transient response tests at a rotational frequency of 34 Hz. For the uncontrolled case, a temporary increase in unbalance caused a persistent jump response involving coupled whirl (Fig. 13(a)). Although the amplitude of rotor vibration did not change significantly, high amplitude vibration of the stator caused large contact force values. With control, amplitude jump was prevented and the rotor returned to the original vibration state (Fig. 13(b)).

These results confirm that the controller design can deal with flexural modes associated with either the rotor or stator structure (or both). They also provide indication that the control methodology may be applicable to systems where control forces are not applied through an active bearing but via other forms of actuation incorporated within the machine structure.

VII. Conclusions

A model-based controller design based on dynamic feedback of measured rotor-stator interaction forces has been developed that is effective in eliminating jump-response modes in the vibration of a nonlinear rotordynamic system. The design approach is able to deal with a number of complicating system features including flexible multi-mode dynamics, noncollocation of actuators and sensors and limited actuator

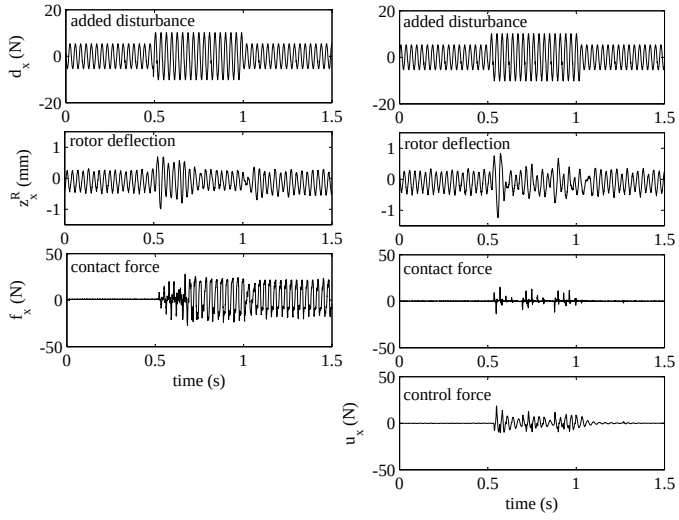

Fig. 13. Experimental transient test at 34 Hz for modified stator dynamics (low frequency stator natural mode). Tests involve temporary increase in unbalance: (a) Uncontrolled case (b) Controlled case

capacity/bandwidth. For industrial application, there are still some issues that would need to be addressed, particularly, how best to integrate sensors in a real machine structure so that rotor-stator interaction forces can be measured for use by the controller. If a number of sensing locations can be incorporated in a stator structure then the controller could deal with multiple potential interaction planes. Such capability may prove useful for improving safety and performance of industrial machines.

APPENDIX A
ROTATING TRANSFORMATION

Under the assumption that the response in the contact plane involves a circular orbit, we may write $\boldsymbol{z}_d(t) = \boldsymbol{T}_\omega(t)\boldsymbol{z}_0$ where $\boldsymbol{z}_0$ is a static vector and $\boldsymbol{T}_\omega(t)$ is a rotation matrix:

$$\boldsymbol{T}_\omega(t) = \begin{bmatrix} \cos\omega t & -\sin\omega t \\ \sin\omega t & \cos\omega t \end{bmatrix} \tag{27}$$

Note that $\boldsymbol{T}_\omega^T\boldsymbol{T}_\omega = \boldsymbol{I}$ and $\dot{\boldsymbol{T}}_\omega = \omega\boldsymbol{\Pi}^T\boldsymbol{T}_\omega$ with $\boldsymbol{\Pi}$ as given in (23). Defining transformed variables $\bar{\boldsymbol{z}} = \boldsymbol{T}_\omega^T\boldsymbol{z}$ and $\bar{\boldsymbol{f}} = \boldsymbol{T}_\omega^T\boldsymbol{f}$ then, from the given form of (6), it follows that

$$\bar{\boldsymbol{f}}^T\dot{\bar{\boldsymbol{z}}} \;=\; \boldsymbol{f}^T\dot{\boldsymbol{z}} + \omega\boldsymbol{f}^T\boldsymbol{\Pi}\boldsymbol{z} \tag{28}$$

Under the assumption $\boldsymbol{e} = 0$, the second term is always zero. Now we may also write $\bar{\boldsymbol{z}} = \boldsymbol{T}_\omega^T\boldsymbol{C}_z\boldsymbol{X} + \boldsymbol{z}_0$ and so $\dot{\bar{\boldsymbol{z}}} = \boldsymbol{T}_\omega^T\boldsymbol{C}_z\dot{\boldsymbol{X}} + \omega\boldsymbol{T}_\omega^T\boldsymbol{\Pi}\boldsymbol{C}_z\boldsymbol{X}$. Thus,

$$\boldsymbol{f}^T\dot{\boldsymbol{z}} = \bar{\boldsymbol{f}}^T\dot{\bar{\boldsymbol{z}}} = \boldsymbol{f}^T\boldsymbol{T}_\omega\dot{\bar{\boldsymbol{z}}} = \boldsymbol{f}^T(\boldsymbol{C}_z\dot{\boldsymbol{X}} + \omega\boldsymbol{\Pi}\boldsymbol{C}_z\boldsymbol{X}) \tag{29}$$

APPENDIX B
LMI TRANSFORMATIONS

Defining, from (24)

$$\begin{bmatrix} \boldsymbol{Q}_{11} & \boldsymbol{Q}_{12} \\ \boldsymbol{Q}_{21} & \boldsymbol{Q}_{22} \end{bmatrix} = \begin{bmatrix} \boldsymbol{P}^{-1} & \boldsymbol{0} \\ \boldsymbol{0} & \sigma^{-1}\boldsymbol{I} \end{bmatrix}^T \mathbb{N}_0(\Omega) \begin{bmatrix} \boldsymbol{P}^{-1} & \boldsymbol{0} \\ \boldsymbol{0} & \sigma^{-1}\boldsymbol{I} \end{bmatrix}$$

With substitutions $\boldsymbol{S} = \boldsymbol{P}^{-1}$, $\boldsymbol{K} = \boldsymbol{L}\boldsymbol{S}^{-1}$, $\zeta = \sigma^{-1}$, $\eta = \nu\sigma^{-1}$ then

$$\begin{aligned}
&\boldsymbol{Q}_{11} = \boldsymbol{A}\boldsymbol{S} + \boldsymbol{S}\boldsymbol{A}^T + \boldsymbol{B}_u\boldsymbol{L} + \boldsymbol{L}^T\boldsymbol{B}_u^T + \boldsymbol{L}^T\boldsymbol{L} + \alpha^2\boldsymbol{S}\boldsymbol{C}_z^T\boldsymbol{C}_z\boldsymbol{S},\\
&\boldsymbol{Q}_{21} = \boldsymbol{Q}_{12}^T = \zeta\boldsymbol{B}_f^T - \eta(\boldsymbol{C}_z\boldsymbol{A} + \Omega\boldsymbol{\Pi}\boldsymbol{C}_z)\boldsymbol{S} - \boldsymbol{C}_z\boldsymbol{S},\\
&\boldsymbol{Q}_{22} = -2\zeta k^{-1}\boldsymbol{I}.
\end{aligned}$$

By a completion of squares argument $\boldsymbol{Q}_{11}$ is minimized with $\boldsymbol{L} = -\boldsymbol{B}_u^T$. Then, by Schur complement, (25) is obtained.

REFERENCES

[1] A. M. Mohamed and I. Busch-Vishniac, "Imbalance compensation and automation balancing in magnetic bearing systems using the Q-parametrization theory," *IEEE Trans. Contr. Syst. Technol.*, vol. 3, no. 2, pp. 202–211, 1995.

[2] D. W. Manchala, A. B. Palazzolo, A.K. Lin, A. K. Kasak, J. Montague and G. V. Brown, "Constrained quadratic programming active control of rotating mass imbalance," *Journal of Sound and Vibration*, vol. 205, pp. 561–580, 1997.

[3] R. Herzog, P. Buhler, C. Gahler and R. Larsonneour, "Unbalance compensation using generalized notch filters in the multivariable feedback of magnetic bearings," *IEEE Trans. Contr. Syst. Technol.*, vol. 4, no. 5, pp. 581–586, 1996.

[4] C. Knospe, R. Hope, S. Fedigan and R. Williams, "Experiments in the control of unbalanced response using magnetic bearings," *Mechatronics*, vol. 5, pp. 385–400, 1995.

[5] K. Nonami and Z. Liu, "Adaptive unbalance vibration control of magnetic bearing system using frequency estimation for multiple periodic disturbances with noise," in *Proc. IEEE Conference on Control Applications*, vol. 1, Kohala Coast, HI, pp. 576–581, 1999.

[6] K.-Y. Lum, V. T. Coppola and D. S. Bernstein, "Adaptive autocentering control for an active magnetic bearing supporting a rotor with unknown mass imbalance," *IEEE Trans. Contr. Syst. Technol.*, vol. 4, no. 5, pp. 587–597, 1996.

[7] H. F. Black, "Interaction of a whirling rotor with a vibrating stator across a clearance annulus," *Proc. IMechE, J. Mech. Eng. Sci.* vol.10, no.1, pp. 1–12, 1968.

[8] M. O. T. Cole and T. Wongratanaphisan, "Synchronous whirl mode maps for rotor vibration with stator interaction across clearance annuli in multiple planes," *Proc. IMechE, Part C: J. Mech. Eng. Sci.*, vol.227, no. 2, 2013, pp. 261–275.

[9] T. Inoue, J. Liu, Y. Ishida and Y. Yoshimura, "Vibration control and unbalance estimation of a nonlinear rotor system using disturbance observer," *ASME J. Vibr. Acoust.*, vol. 131, art. no. 031010, 2009.

[10] M. O. T. Cole and P. S. Keogh, "Rotor vibration with auxiliary bearing contact in magnetic bearing systems, part 2: robust synchronous control to restore rotor position," *Proc. IMechE, Part C: J. Mech. Eng. Sci.*, vol. 217, no. 4, pp. 393–409, 2003.

[11] L. B. Ginzinger, *Control of a rubbing rotor using an active auxiliary bearing*, Ph.D. dissertation, 2009, Technical University Munich.

[12] I. S. Cade, M. N. Sahinkaya, C. R. Burrows and P. S. Keogh, "An active auxiliary bearing control strategy to reduce the onset of asynchronous periodic contact modes in rotor/magnetic bearing systems," *ASME J. Eng. Gas Turbines and Power*, vol. 132, no. 2, art. no. 052502, 2010.

[13] A. Simon and G. T. Flowers, "Adaptive disturbance rejection and stabilisation for rotor system with internal damping," *International Journal of Acoustics and Vibrations*, vol. 13, no. 2, pp. 73–81, 2008.

[14] M. Karkoub, "Robust control of the elastodynamic vibration of flexible rotor system with discontinuous friction," *ASME J. Vib. Acoust.*, vol. 133, art. no. 034501, 2011.

[15] M. N. Sahinkaya, and C. R. Burrows, "Control of stability and the synchronous vibration of a flexible rotor supported on oil-film bearings," *ASME J. Dyn. Syst., Meas., Control*, vol. 10, pp. 139–144, 1985.

[16] A. El-Shafai, A. S. Dimitri, "Controlling journal bearing instability using active magnetic bearings," *ASME J. Eng. Gas Turbines Power*, vol. 132, no. 1, art. no. 012502, 2010.

[17] M. O. T. Cole, C. Chamroon, P. Ngamprapasom, "Force feedback control for active stabilization of synchronous whirl orbits in rotor systems with nonlinear stiffness elements," *ASME J. Vib. and Acoust.*, vol. 134, no.2, 021018, 2012.

[18] Schweitzer, G., Maslen, E. (Eds.), Chapter 10, *Magnetic Bearings*, Berlin: Springer, 2010.

[19] M. O. T. Cole, "On stability of rotordynamic systems with rotor-stator contact interaction," *Proc. R. Soc. A.*, vol. 464, no. 2100, pp. 3353-3375, 2008.

[20] S. Boyd, E. Feron, L. E. Ghaoui and V. Balakrishnan, *Linear Matrix Inequalities in System and Control Theory*, Pennsylvania: SIAM, 1994.

[21] H. K. Khalil, *Nonlinear Systems*, New Jersey: Prentice Hall, 2000.